Asteroid Centrifugal Fragmentation

Final Report

Authors: Michel P., Walsh K.
Affiliation: Côte d'Azur Observatory, University of Nice-Sophia Antipolis, France

ESA Research Fellow/Technical Officer: **Claudio Bombardelli, Dario Izzo**

Contacts:

Patrick Michel
Tel: +33(0)492003055
Fax: +33(0)492003058
e-mail: michel@oca.eu

Dario Izzo
Tel: +31(0)715658718
Fax: +31 71 565 8018
e-mail: act@esa.int

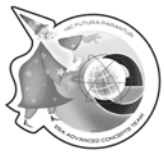

Available on the ACT website
http://www.esa.int/act

Ariadna ID: 07/4111
Study Duration: 6 months
Contract Number: 20782/07/NL/CB

1. INTRODUCTION

MOTIVATIONS AND ASSUMPTIONS

Among the properties of small Solar System bodies, spin is important as it gives clues about some of the body's internal physical properties. Indeed, the equilibrium shape of a body under a given spin depends on its internal structure (see e.g. Holsapple 2007). Thus, it is well known that above a certain limit, which depends on a few physical parameters, the body cannot survive in its original state. It must either readjust to another shape, or break if the spin value gets too high. This consideration is at the origin of the space mission concept aimed at spinning up a small body to break it (e.g. for mitigation) or release some material and open some internal areas (as a way to investigate its internal properties). However, to determine whether such a concept would be effective, one must first characterize the potential outcomes of such rotational fragmentation: Do the fragments fly away or is there a possibility that a binary or a multiple system is produced? And what are the body's needed properties (e.g. its strength) for either of these outcomes to occur? Then, how much time is necessary for a shape change of the body and then for the escape of a piece of material from the surface, as a function of the initial spin and the applied spin increase? The aim of this report is to address these questions. Note that there is a natural process called the YORP effect (see further) which can increase the spin rate of small rocky bodies, and which can eventually lead to their break-up. Thus, this problem is not only interesting in the framework of a space mission definition, it is also a crucial scientific problem, as rotational break up is expected to be a natural process in our Solar System.

The spin at which a body breaks and the outcome of the disruption are strongly influenced by the body's strength. Section 2 recalls the different kinds of strength that are relevant to rocky bodies. These are, essentially, the tensile, compressive and shear strengths. However, there is strong evidence that asteroids with sizes above a few hundreds of meters are likely to be cohesionless bodies, which means that they have no tensile strength. Furthermore, bodies larger than a few kilometers (maybe even smaller, down to a few hundreds of meters) have a negligible tensile strength, and thus a model of cohesionless bodies for large asteroids is also reasonable (see Holsapple 2007 for justification). Note that it is common to equate "zero tensile strength" to a fluid body, but that is not correct. A granular material such as dry sand can withstand considerable shear stress if it is under pressure: that is why one can walk on dry sand but not on water. But dry sand has no tensile strength. Therefore, zero tensile strength does not mean "fluid". The confining pressure, in the case of asteroids, is due to the self-gravity, and thus such a model of a cohesionless body is appropriate for bodies whose gravity dominates over its tensile strength. Such bodies are also commonly called rubble piles or gravitational aggregates (see Richardson et al. 2002 for a detailed definition).

Significant evidence exists suggesting that asteroids down to a few hundreds of meters in diameter are gravitational aggregates. On the observational side, the bulk density derived from space mission visits to a few asteroids (e.g. the NASA mission NEAR that visited the asteroids Mathilde and Eros, the JAXA mission Hayabusa that visited Itokawa) are always smaller than the grain density of meteorite equivalents. Thus, a great amount of porosity (between 20% and 40%) is estimated to characterize these bodies. The most striking example is the asteroid Itokawa, which, despite its small size (average diameter of ~320 meters), has a bulk density of 2 g/cm^3, which gives it a porosity of 40% (Fujiwara et al. 2006, Abe et al.

2006). Such a value is greater than the porosity of sand and about as loose as one can possibly pack a rock pile. This is the first direct evidence that bodies as small as 300 meters can be gravity-dominated. Moreover, spin measurements are also consistent with the fact that asteroids in this size range and above can be modeled as gravity-dominated bodies. Indeed, a theoretical study performed by Holsapple (2007) showed that bodies larger than a few kilometers have a spin limit corresponding to that of cohesionless bodies, even if they may be monolithic, because the tensile strength of large bodies is negligible anyway compared to gravity. Such a limit is consistent with the one observed. Moreover, at smaller sizes, bodies can spin faster (in agreement with observations), and only a very small cohesion (in the range of a few KPa) is needed for them to survive at those spins. So, these small bodies may still consist of rubble piles with only a small amount of cohesion between some of their components.

Such results agree with those obtained from numerical simulations of catastrophic disruptions of asteroids. Benz and Asphaug (1999) estimated the impact energy per unit target mass required to break a body so that the largest fragment contains exactly 50% of the original mass (called the catastrophic impact energy threshold or Q^*_D). Using monolithic targets composed of basalt or ice material, they found that for targets in the size range from a centimeter to a few hundreds of meters, the required energy decreases with the body's size. This is because in this size range (called the strength regime), the outcome is controlled by the material (tensile) strength, and this strength decreases with the size of the body due to the greater likelyhood of pre-existing large natural faults in a large body, reducing its strength. Then, above a few hundreds of meters, the required energy starts increasing with the body's size, because gravity starts dominating. Thus, even on the theoretical/numerical side, it is found that bodies as small as a few hundreds of meters can be gravitational aggregates.

Obviously, some of these bodies may still be monolithic, and there is certainly a size limit below which small bodies are expected to be monolithic, but this limit for asteroids is still a subject of large debates in our community. Nevertheless, in this report we propose to address the problem of rotational fragmentation for bodies consisting of gravitational aggregates. One reason comes from the evidence indicated previously. However, it limits our study to bodies whose size is at least a few hundreds of meters. The second reason is a technical one. The rotational break up of a monolithic body requires the explicit computation of its fragmentation by the propagation of cracks, since a monolithic body has a non-zero tensile strength. Thus, when the spin of such a body increases, the tensile stress increases and can eventually reach the threshold for crack activation. The dynamics of the process is in this case governed by the production of fragments by the crack propagation and must therefore be addressed by appropriate numerical models. The state-of-the-art numerical code of fragmentation for planetary science developed by one of us (W. Benz) is based on the Smoothed Particle Hydrodynamics (SPH) technique (see e.g. Benz and Asphaug 1994), and as we will explain in Sec. 3, unfortunately it cannot accurately handle rotating bodies in its current version. Only very recently has a correction been proposed that should allow in principle the study of rotating bodies in this regime, but further tests are necessary. So, as a first step, we only consider gravitational aggregates whose break up by rotation is purely controlled by their gravity. Then, there is no need for these bodies to compute their fragmentation by crack activations. Since they are believed to accurately represent the bodies whose size is larger than a few hundreds of meters, such a study provides a great contribution to improve our knowledge of this problem.

The remainder of this report is divided as follows. Section 2 describes some concepts about the strength of a small rocky body. Section 3 briefly discusses the model of fragmentation generally used to compute the crack propagation within a rocky body. This model is implemented in hydrocodes for simulating the disruption of an asteroid due to an impact with a projectile. We will then explain in the same section the reason why we could not simulate the disruption of a rotating body with our hydrocode based on the SPH numerical techniques, therefore limiting the study to gravity-dominated bodies. Section 4 details our numerical model and Section 5 explains the results. Conclusions and perspectives are providedin Section 6.

2. SOME DEFINITIONS AND CONCEPTS ABOUT MATERIAL STRENGTH

The term ”strength” is often used in imprecise ways, and it is important that this concept is well understood. The description provided here is largely taken from Holsapple & Michel (2006) and Holsapple (2006). Materials such as rocks, dirt and ice, of which small bodies of our Solar System are made, are complex and characterized by several kinds of strength. Generally, the concept of ”strength” is a measure of an ability to withstand stress. But stress, as a tensor, can take on many different forms. One of the simplest is a uniaxial tension, and this tensile strength is often (mis)used to characterize material strength as whole. Thus, while it is common to equate ”zero tensile strength” with a fluid body, that is not correct. In fact, while a ”fluid” can have zero tensile strength, ”solids” may also. For instance, dry sand has no tensile strength. However, dry sand and granular materials in general can withstand considerable shear stress when they are under pressure: that is why we can walk on dry sand but not on water. Here comes into play a second kind of strength: the shear strength, which measures the ability to withstand pure shear. The shear strength in a granular material under confining pressure comes from the fact that the interlocking particles must move apart to slide over one another, and the confining pressure resists that. Then a third kind of strength, the compressive strength, governs the ability to withstand compressive uniaxial stress. Thus, a general material has tensile strength, shear strength at zero pressure (technically the ”cohesion”) and compressive strength. In geological materials such as soils and rocks, the failure stresses depend strongly on the confining pressure; as a result, these three strength values can be markedly different. A cohesionless body, such as what is considered in this report, is simply a solid body whose cohesion (shear strength at zero pressure) is zero, but that does not mean it does not have any shear strength under confining pressure (provided by the self-gravity). Hence, a body can be cohesionless but nevertheless solid (non-fluid).

The Drucker-Prager (DP) model is a common model for geological materials, as is the Mohr-Coulomb criterion (MC) (the difference between these two models is not relevant for our study). The DP model assumes that the allowable shear stress[1] depends linearly on the confining pressure. Physically that is the consequence of the interlocking of the granular particles, and not the friction on the surfaces of the particles; although the model behaves like models for linear friction[2]. The DP model is defined by two constants: one defines the

[1] More precisely, the square root of the second invariant of the deviator stress. That measure is the shear stress if the stress state is simply a pressure plus a single shear stress.

[2] The shear strength in a granular material under confining pressure is due to the fact that the interlocking particles must move apart to slide over one another, and the confining pressure resists that. A closely packed mass of uniform rigid *frictionless* spherical particles in a uniform gravity field has an angle of friction of about 23° (Albert et al. 1997), so the term angle of *friction* is somewhat of a misnomer. Angle of *interlocking* might be better.

"cohesion" (shear strength at zero pressure); and the second defines the dependence on the confining pressure: that constant is related to what is called the "angle of friction" in geo-mechanics. Those two values then determine the tensile and compression strengths.

In studies of the mechanics of Solar System bodies, it is nowadays generally believed that the effective cohesive strength decreases with increasing body size. That is a consequence of the increasingly large sizes of faults, cracks and other defects, which determine the strength. At the same time, the self-gravitation pressure increases with size. Therefore, at some size the pressure gravity effects dominate the cohesive strength effects, and the cohesion can be ignored. For example, in cratering mechanics there is the "strength regime" for small craters, where cohesive strength matters, and the "gravity regime" for large craters, where the cohesive strength does not matter (see for example, Holsapple 1993). In the catastrophic disruption of bodies by impacts, the same is thought to be true (see, for example, Holsapple et al. 2002 and Benz and Asphaug 1999). For the spin of ellipsoidal bodies, Holsapple (2007) determined that the cohesive strength has negligible effect compared to the gravity forces for bodies over a few kilometers in diameter, but we also have evidence that bodies as small as a few hundreds of meters may be cohesionless. For that reason, it is appropriate to ignore the cohesion as a first step in this study. This means that there is also no tensile strength: instead our asteroid model consists of large number of particles that can withstand shearing forces as a consequence of its gravitational pressure. It is a body of dry sand or an assemblage of rocks, gravel and cobbles (modeled as hard spheres).

3. MODEL OF FRAGMENTATION

This section could be considered as an addendum to this report as it is independent of other ones. Indeed, although our report only addresses the rotational disruption of gravity-dominated bodies, for which material strengths can be neglected and which allows using a model that does not account for any crack propagation, one could also be interested in studying this problem for small monolithic bodies. In such a case, the fragmentation involves the propagation of cracks due to their activation by stress increase as a result of the spin-up. In this section, we briefly describe the model of fragmentation of brittle materials generally used to compute such processes as a result of the impact of a projectile. We refer the reader to the article by Benz and Asphaug (1994) for details. Then we show at the end of this section why this model, when introduced in Lagrangian hydrocodes based on SPH techniques and when considering a rotating body, is confronted by some problems that need further investigation.

3.1 ELASTIC-PERFECTLY PLASTIC STRENGTH MODEL

The most commonly used fracture model is derived from a continuum model of fragmentation developed by Grady and Kipp (1980). It is based on the assumption that a brittle solid contains an initial distribution of incipient flaws, supposed to be represented by a Weibull distribution (Weibull 1939). This is a probability distribution that defines the most likely number of flaws per unit volume having failure strains lower than ε by the power law:

$$n(\varepsilon) = k\,\varepsilon^m,$$

where k and m are material constants called the Weibull coefficients. These parameters have been measured for a number of geological and industrial materials, including basalt

(Nakamura et al. 2007), although data are still scarce for some important rocks that may well represent asteroids. Cracks evolve in a solid when Weibull flaws activate, i.e. when their failure strain is exceeded, and grow at some fraction of the sound speed. Grady and Kipp model local stress release due to the growth of cracks with a state variable D (for "damage") that goes from 0 to 1, and which is derived from the Weibull distribution and strain history. Damage expresses the reduction in strength under tensile loading. The reduction in stress is expressed as:

$$\sigma_D = \sigma (1- D)$$

where σ is the elastic stress in the absence of damage and σ_D is the damage-relieved stress. A material with sufficient cracks to have a damage D=0.5 feels half the stress it would otherwise feel under the same tensile strain. A fully damaged material feels no tensile stress whatsoever, and thus such material would be considered as a fully damaged cohesionless body, explaining why we do not need such a model to address the disruption of cohesionless bodies. In more than one dimension, the equation above is replaced by the following relationship between the stress tensor σ_{ij} and the strain tensor ε_{ij}:

$$\sigma_{ij} = -P^* \delta_{ij} + (1-D) S_{ij},$$

where $P^* = P$ if $P > 0$ (P being the pressure) or $P^* = (1-D) P$ if $P < 0$ and S_{ij} is the deviatoric stress tensor (non-diagonal part).

In the Grady-Kipp model, damage is a state variable: it is equal to the fractional volume that is relieved of stress by the network of growing cracks. The Weibull distribution being a number density, damage is best viewed as a dimensionless volume density. A crack relieves stresses in a neighborhood approximately equal to a circumbscribed sphere (Walsh 1965), such that damage in a volume V with a single crack in it of half length a is:

$$D = (4 \pi a^3) / (3 V).$$

Grady and Kipp assume that cracks grow at a constant velocity c_g, so that the half-length of a growing crack is:

$$a = c_g (t-t'),$$

where t' is the crack activation time. The crack growth speed is a fraction of the speed of a longitudinal elastic wave (Lawn and Wilshaw 1975), generally assumed to be about 0.4. If the damaged volume is a sphere of radius R_s and a single crack is propagating in it, then the differential form for the cube root of damage is expressed as:

$$d D^{1/3} / dt = c_g / R_s.$$

Under an increasing strain, increasing numbers of Weibull flaws activate in succession, with different crack lengths. Damage becomes an integral over all these growing cracks. Grady and Kipp approximate this integral with the differential equation:

$$d D^{1/3} / dt = [(m+3) \alpha^{1/3} \varepsilon^{m/3}]/3,$$

where

$\alpha = 8 \pi c_g^3 k / [(m+1)(m+2)(m+3)]$

which allows damage to grow monotonically in a realistic manner when strain rate varies with time. By solving stress as a function of time and setting its derivative to zero, Grady and Kipp derive the dynamic tensile strength of a material:

$\sigma_T = [3E (m+3) \ d\varepsilon/dt] / [(m+3)(m+4)^{-(m+4)/(m+3)} \alpha^{-1/(m+3)}]$

where E is the elastic modulus of the undamaged material. If $d\varepsilon/dt \rightarrow 0$ the material becomes strengthless. This reflects the fact that theirs is a dynamical model and should only be applied at high loading rates; in practice, one takes σ_T to be the maximum of the value given by the expression above and the static strength.

To compute the evolution of the damage propagation as a result of a stress increase in a solid body, the equations to be solved are the well-known conservation equations of hydrodynamics and can be found in standard textbooks. Then, a basic Hooke's law model is assumed in which the stress deviator rate is proportional to the strain rate. Provided that an equation of state links the pressure to the density and internal energy, this set of equations can be solved and describes a perfectly elastic material. Then, the plastic behavior, which represents the fact that a critical stress always exists that results in permanent deformation, can be introduced in the equations. Generally, a von Mises criterion is used to limit the deviatoric stress tensor. Then the fracture model described above is used to compute the crack propagation.

3.2 PROBLEM WITH ROTATING TARGETS

While the fracture model derived in the previous subsection may be implemented in any Lagrangian finite-difference hydrocode, the SPH method provides a very natural framework that is highly suitable to the propagation of fractures and the formation of fragments. Extensive reviews on this method exist in the literature (see e.g. Benz 1990, Monaghan 1992). The state-of-the-art hydrocode originally developed by Benz and Asphaug (1994), which was used to obtain most current results on asteroid disruption, is based on SPH techniques. However, bodies were always considered to be non-rotating in those previous studies, because SPH was not able to accurately handle rotating targets. This is not necessarily a big problem for studying the disruption of an asteroid by impact, but it prevents its use to study the rotational fragmentation of an asteroid.

The reason why standard SPH is unable to handle the rotation of solid bodies accurately is that particle disorder leads very quickly to large errors in the computation of the spatial derivative of the stress tensor. These errors feed back into the time evolution of the system and lead rapidly to completely erroneous results. As shown by Speith (2008), a correction term can be computed which ensures first-order consistency resulting in a cancelation of the errors due to particle disorder.

To illustrate the problem, a simple rotation of a solid cylinder around its long axis (z.axis) has been simulated. Fig. 1 shows the time evolution of the angular momentum of the cylinder as a function of time. In half a turn, the cylinder simulated with standard SPH (solid line) has lost its entire angular momentum and begins to rotate in the opposite direction! On the other hand, the corrected version of SPH is capable of following the cylinder's rotation (dashed line) without significant loss of angular momentum. Figs. 2 and 3 show particles and the associated

velocity vectors in an equatorial slice after 0.8 rotation period. The fact that the uncorrected version of the code leads to a cylinder rotating in the opposite direction is clearly visible.

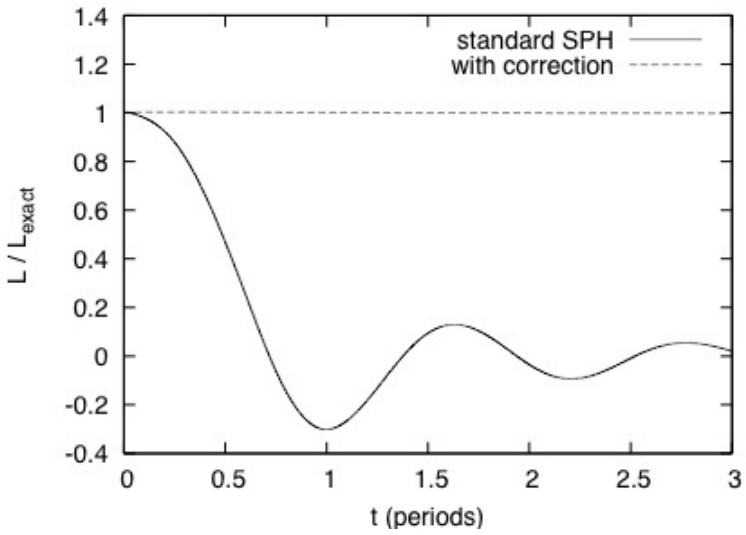

Figure 1: Time evolution of the angular momentum of a rotating cylinder, computed with the standard SPH and with the corrected version.

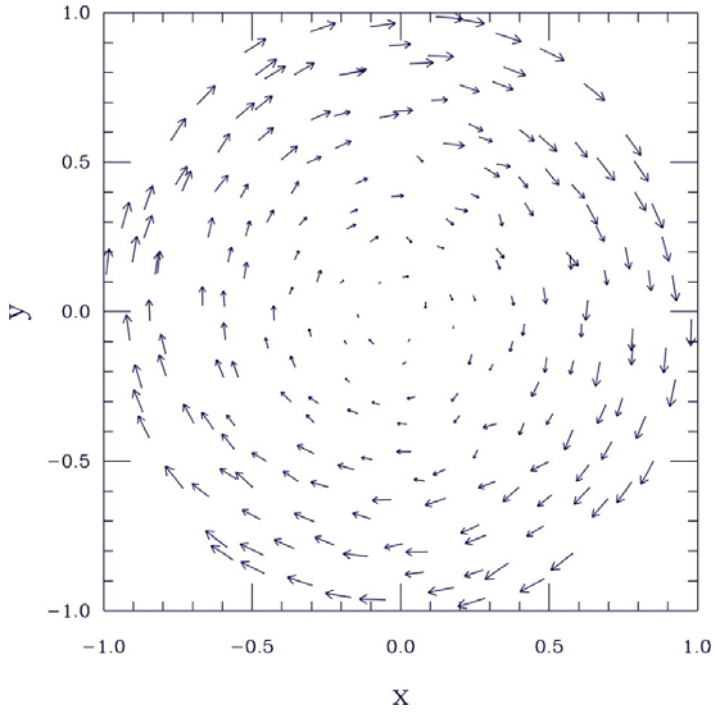

Figure 2: Particles and the associated velocity vectors in an equatorial slice of the cylinder after 0.8 rotation period computed with the standard version of the SPH hydrocode.

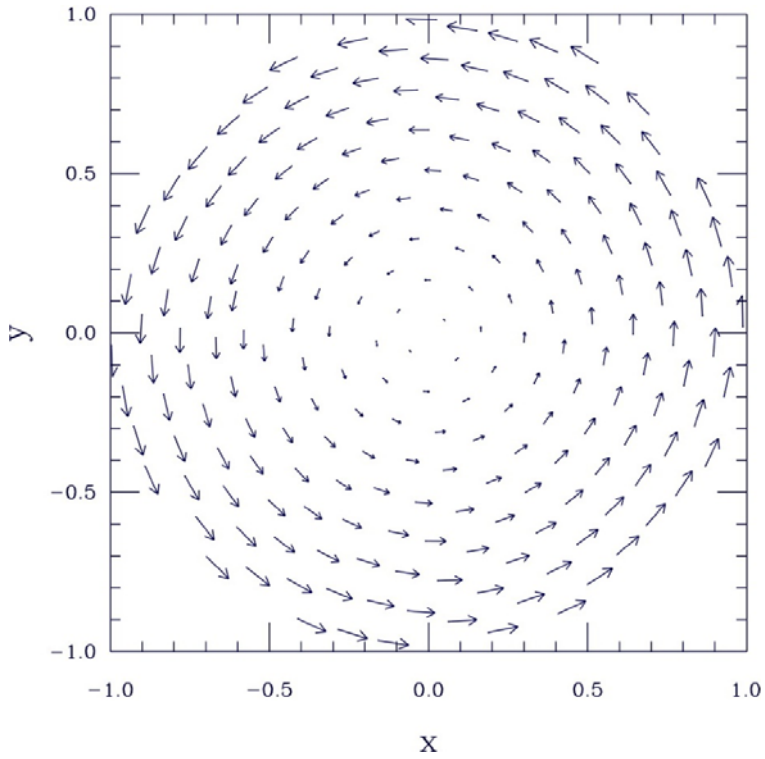

Figure 3: Particles and the associated velocity vectors in an equatorial slice of the cylinder after 0.8 rotation period computed with the corrected version of the SPH hydrocode.

Therefore the proposed correction looks promising. However, it has not been fully tested, and to apply it with confidence to the study of rotational fragmentation of a strength-dominated body would require an amount of work that cannot be accomplished on the timescale allocated for this report.

In this report, because of the current inability of SPH hydrocodes to handle rotation, and because of the evidence that gravity-dominated bodies are likely to be the norm among members of the asteroid population whose sizes exceed a few hundred meters, we consider only this last kind of body to address the problem of rotational disruption. Our numerical method is presented in the next section, followed by the results of our investigations.

4. ROTATIONAL DISRUPTION OF COHESIONLESS BODIES

4.1 OUR ASTEROID MODELS

A. N-body model

Many lines of evidence suggest that most asteroids between 200 m and 50 km in diameter are likely rubble piles, or gravitational aggregates (see above and also Richardson et al. 2002). This means that the bodies are assemblages of rocks held together by self-gravity, rather than being coherent monoliths. Despite many unknowns about the internal configurations and structures of rubble piles, many of their observed properties have been matched quite well with *N*-body simulations, such as for instance the accurate model of the Shoemaker-Levy 9 tidal disruption at Jupiter (Asphaug & Benz 1994).

The *N*-body code that we use, called `pkdgrav`, is an hierarchical tree code based on a symplectic leapfrog integration routine and is parallelised. The tree allows for significant increases in the speed of integration, at the cost of small errors in force accuracy, making timestep selection important (smaller steps reduce the effect of the force errors, which tend to be randomly, not systematically, distributed). The specifics of the tree are controlled via a parameter called the opening angle, which determines which nodes are opened for direct gravity calculations, and determines the overall speed and accuracy of the calculation. The code has been well-tested in a wide array of environments (see Richardson et al. 2000 and Richardson et al. 2008). More details were provided in the proposal document of this project.

Within the integrator, collisions between particles are searched for using a tree: a configurable-number of nearest particles are checked for possible collisions during the next timestep. Multiple collisions among particles during the step are handled correctly. When two particles collide their resulting trajectories and velocities are determined using simple formulae for the mutual rebound of two hard spheres. For impacts where the relative speed of the two particles is above 10% of their mutual escape speed, the ratio of rebound speed to impact speed is controlled by the parameter called the coefficient of restitution. Below 10% of their mutual escape speed, the collisions are perfectly elastic. Thus each rubble pile, represented by a group of self-gravitating hard spherical particles, is constantly in a state of low-energy excitement, with particles lightly bouncing off one another. Without this effect the piles would collapse into a numerically unstable state.

B. Rubble Piles

i. Rubble Pile Creation

For our nominal case represented by a monodisperse population of particles (all particles having identical size and mass), each initial rubble pile is started in a close-packed formation. Variations of this scenario are used throughout this study, so the fundamental geometry is important to discuss. The limiting density for packing of spheres is given by hexagonal closest packing (HCP). This packing results in a minimum void space of ~26% (see Leinhardt et al. 2000). When creating a rubble pile for simulations, the spheres are packed in HCP with 1% of particle radius space between each particle. Each particle is then given a random velocity vector with 1% of the particle's escape speed. This immediately puts each rubble pile into a state of excitement for which it is numerically stable, but is well below the energy required to reshape the pile. The other benefit of this creation scenario is that each generated rubble pile is different, despite similar physical properties and initial packing formation, as the initial velocities are random for each.

Variations on the nominal case of HCP are used for different initial rubble formations, as not every rubble pile tested begins with a monodisperse population of particles. Most variations rely on using the original geometry of HCP, but with very large initial particle separations followed by a period of collapse, allowing for a random reconfiguration of the spheres. This method of rubble pile formation was used for all bi-modal particle distributions (two different particles sizes), and for placing surface particles around a rigid core.

For many simulations a rubble pile with an initial elongation was used as an initial condition. For all but the nominal case (where we can pack spheres into an ellipsoidal shape), the rubble piles were created by allowing a collapse of particles into a random configuration. In these

collapse scenarios the bodies always end up as nearly spherical. To create an elongated rubble pile for these cases it is necessary to initially create a large body with ~2000 particles. Then a routine is used to "carve" out an ellipsoid with the required shape, leaving ~1000 particles in an elongated, and randomly configured rubble pile.

ii. The Nominal Rubble Pile

As described above, the nominal rubble pile in these simulations was one with identical spherical particles, in an initially excited hexagonal closest packing formation. For all simulations the particle density is 3.4 g/cc, which means the bulk density for the nominal case is ~2.3 g/cc. Spin tests done by Richardson et al. (2005), using the same code, showed that a monodisperse rubble pile behaves similarly to a cohesionless granular material with an angle of friction (ϕ) ~40°.

iii. The Fluid Case, $\phi \sim 0°$

A rubble pile that possesses many fluid properties was created using a bi-modal particle distribution. Using the rubble pile creation mechanism explained above, 33% of the ~1000 particles were randomly increased in size by 25% (mass was also increased to keep particle density constant). Then the cloud of particles collapsed into a rubble pile that was randomly organised. The bulk density of the final rubble pile was 2.0 g/cc.

The estimate of the angle of friction of this rubble pile was derived from a spin test, similar to those performed for the nominal monodisperse case by Richardson et al. (2005). These tests simply impart an initial spin on rubble piles of different initial elongations (ratio of the long axis to the short) and measure the resulting outcome (mass loss, reshaping, etc.). The final spin state and rubble pile shape/elongation is then compared to the classical fluid-equilibrium shapes, as well as the limits derived for cohesionless granular material (Holsapple 2001, 2004). For the case of a bimodal rubble pile, regardless of its initial shape or spin, it quickly evolves directly to a fluid equilibrium state. The most dramatic examples of this interesting behavior were cases of low spin-rate (9 h), and moderate elongation (*a:c*) (1.7:1). This shape/spin configuration is stable for even very modest angles of friction, but these rubble piles quickly evolved to a new state with a 7.75 h rotation period and an axis ratio of 1.5:1.14 (see Fig. 4).

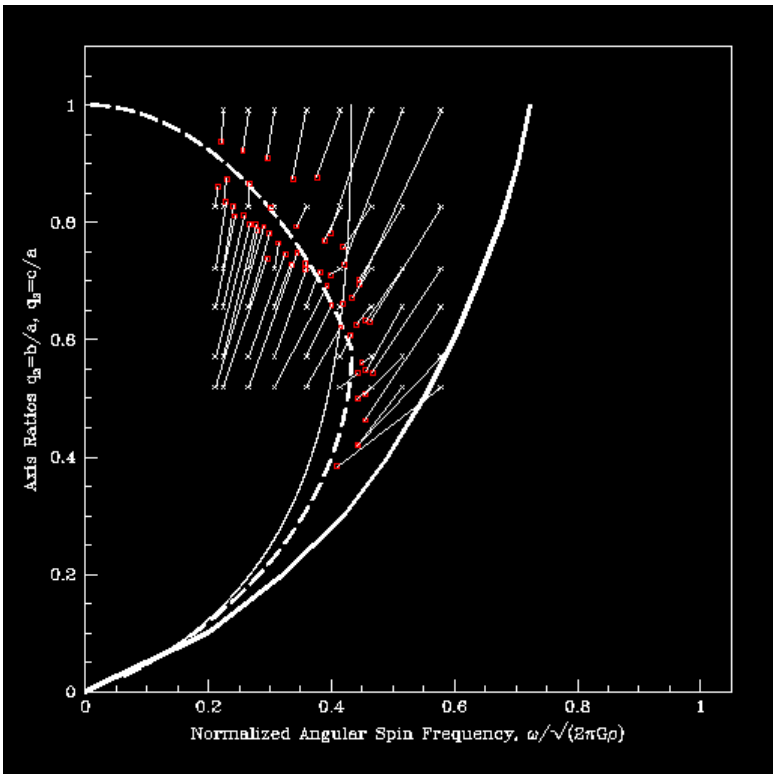

Figure 4: Axis ratios as a function of normalized spin frequency of bodies whose initial spin is imparted. The crosses indicate the initial spins and shapes. The red squares indicate the final states of equilibrium which are all close to one of the two equilbrium lines for fluid bodies indicated by the dotted and thin full lines. The thick full line indicates the equilibrium solutions for a cohesionless body with a 40° angle of friction.

iii. Intermediate Case, $\phi \sim 20°$

The intermediate angle of friction used for simulations was for a rubble pile with a value ϕ~20°. This rubble pile had a bi-modal distribution of particles, similar to the fluid case, but in this case 33% of the particles were made only 5% larger than the standard particle. Similarly, the rubble pile was created using a cloud of particles that was allowed to collapse under gravity, creating a random configuration of the particles with a final bulk density ~2.0 g/cc.

The spin tests performed on these rubble piles confirm behavior consistent with an angle of friction near 20°. The piles starting with slow spins and moderate elongations were able to maintain their shapes. However the piles starting with elongation/spin configurations beyond the 20° cohesion-less limit suffered shape changes. Those that started well beyond the 20° cohesionless limit suffered major shape changes and evolved back to the classical fluid shapes.

iv. Rubble Piles with Cores

A final test case involved rubble piles not easily characterised by angle of friction estimates. In this case we made rubble piles with a core of particles that were twice as large as the surrounding smaller particles. These core particles were placed in HCP formation, and a cloud of the smaller particles was then collapsed on top in a random configuration. Bodies

with different sized cores were created, one with 25% and 38% of the mass in the core. The real asteroid Itokawa, visited by the JAXA space mission Hayabusa and whose average diameter is about 320 meters, may consist of such kind of large boulder(s) surrounded by smaller ones.

v. High Resolution Tests

To check the simulations' sensitivity to component size, tests were run at varying resolution (different number of particles). At high resolution, due to the computational expense, only small subsets of the simulations performed at the standard resolution of 1000 particles were carried out. Overall, tests were run for cases ranging from 50 to 5000 particles. In general we found little change to our results within the wide range of resolution tested, and therefore we do not discuss these results in detail.

4.2 MODELING SPIN-UP

Modeling a gradual spin-up of a rubble pile asteroid presented a need to alter the standard usage methods of our *N*-body code, and also the creation of new codes. The desired scenario is for a continuous and small increase of the body's angular momentum, affecting the entire body simultaneously, but not any ejected particles. With the basic `pkdgrav` package, adding such an effect is non-trivial, and instead a code was written to run `pkdgrav`, stop the simulation to analyze the state of the body/system and increase the spin rate as needed/desired. So for our model, angular momentum was increased in small discrete "boosts."

The two parameters governing the process are the delay between spin boosts, and the magnitude of these boosts. After a series of tests to determine parameters that are both computationally expedient and which show a convergence in results, delays of 2000 timesteps and angular momentum increases of 1% were used. The delay of 2000 timesteps is roughly five spin periods.

A. Basic Integration Parameters

The basic parameters governing the integrations of the rubble piles are quite similar to those used in past simulations for tidal disruptions and rubble pile collisions (Walsh & Richardson 2006, 2008; Leinhardt et al. 2000). The timestep for each simulation was 10^{-5} yr/2π (50 s), which is less than 2% of each particle's dynamical time. Simulations were run for 2×10^6 timesteps in most cases, and sometimes extended to 3×10^6 timesteps.

The normal coefficient of restitution, the main parameter used to govern collisional outcomes between particles, was an important parameter in these simulations, varying from 0.2 to 0.8. The tangential coefficient of restitution is what would govern "sliding friction" and would allow angular momentum transfer from particle to particle. While this parameter is only used for works with spherical particles, it was not used. Indeed, it is a poorly constrained parameter and somewhat artificial since real particles are not expected to be perfectly spherical.

B. Modeled spin-up in relation to the YORP effect

The spin-up of an asteroid can be artificially performed in the context of a space mission designed for this purpose. Nevertheless, a natural mechanism widely attributed with imparting

drastic spin-state changes on small bodies is the YORP-effect, which arises from reflection and/or absorption and re-radiation of sunlight by the surface of an irregularly shaped asteroid (Rubincam 2000, Paddack 1975). This effect accounts for the rotation-rate increase of NEAs 2000 PH_5 (now re-named YORP) and 1862 Apollo (Lowry et al 2007, Taylor et al 2007, Kaasalainen et al. 2007). The timescale for YORP spin alteration depends on the size R of the body (increasing with R^2), the distance a from the Sun (increasing with a^2), the body's thermal properties, and the body's shape and obliquity. The YORP spinup/spindown timescale for kilometre-size NEAs and MBAs is estimated to be between a few 10^4 and 10^6 yrs depending on the shape and makeup of the asteroid (Rubincam 2000, Cuk 2007). Due to a notable abundance of both fast and slow rotators among NEAs and SMBAs, this effect appears to act widely (Pravec & Harris 2000, Rubincam 2002). However, these timescales are orders of magnitude higher than the ones that could be reached by a space mission to cause a rotational fragmentation.

The YORP effect depends heavily on an asteroid's shape, surface/thermal properties and also its obliquity. Our simulations model $2x10^6$ 50 sec timesteps, covering a total time of ~3.2 yrs. This overall simulation time is drastically shorter than a true YORP timescale, but due to the computational expense, a simulation at the correct physical timescale is effectively impossible with current computing facilities. However, the spin increase is so small over the entire YORP timescale that artificially accelerating the spin-up process is unlikely to negatively affect the outcome. To test this hypothesis, hundreds of simulations were run varying over an order of magnitude the parameters defining the spin-up process, namely the length of time between spin-boosts, and the magnitude of each spin-boost. The standard values used are 2000 timesteps in between each spin-boost, and a spin-boost that increases the spin-period (in hours) by 1%. Values of 200-20,000 timesteps were tested for the delay, and percentages from 0.1-2.5% were tested for spin-boost strength. It was determined that the standard values provide a spin-up which allows for the body to equilibrate in between spin-increases, and is small enough to not initiate mass-loss instantaneously. Mass loss events and re-shaping occur equally spread throughout the simulation, and not directly following a spin-increase. This is also a good representation of what will happen if a space mission is designed to spin-up a small body, even at faster spin-up.

4.3 ANALYZING THE RESULTS

A. Spin and Shape Changes

The spin and shape of the body (the entire body, or the largest remnant after mass has been ejected), were analyzed throughout the simulation. The shape was monitored simply by calculating the lengths of the principal axes, *a*, *b* and *c* (from longest to shortest). The density of the body was calculated by fitting a tri-axial ellipsoid around the body and then calculating the mass inside of this ellipsoid and the volume of the ellipsoid.

B. Orbit Analysis for Ejected Material

In nearly all simulations, the body was spun-up beyond the point where particles were ejected from the surface. At this point in the simulation, the spin-up procedure only applies to the largest body, and additional analyses are made. The shape, spin and density of the main body and the largest orbiting mass are calculated, as well as the amount of mass ejected from the system, and the amount still bound to the main body. The orbital properties of the largest orbiting mass are analyzed with the program `companion` (Leinhardt et al. 2005).

5. DESCRIPTION OF SIMULATIONS

In this section we describe the simulations performed, including the variations selected for rubble piles and important parameters. For the nominal case of the monodisperse rubble pile, the differences between each rubble pile is strictly in the random velocities imparted on each particle, but for the other cases the actual configuration of particles in the initial rubble pile is different from one rubble pile to the other.

5.1 NOMINAL CASE

For the nominal case we used the mono-disperse rubble piles as described above, and started with two initial shapes: spherical and prolate. The prolate body had axis ratios of 2:1:1, where the long axis, *a*, was twice as long as the intermediate, *b*, and short axis, *c*. For each shape, simulations were run with 4 different normal coefficients of restitution: 0.2, 0.4, 0.6 and 0.8. The initial spin rate for this nominal case is 4.4 h, which is within the spin limits for a cohesionless granular material with an angle of friction ~40°.

5.2 STRUCTURE/MATERIAL VARIATION

The other test cases involve the variant rubble pile structures described above: a ~20° angle of friction (intermediate case), ~0° angle of friction (fluid-like case), and those with a rigid core of either 25% of the mass or 38% of the mass. Other parameters remained the same, except for the fluid-like and intermediate cases, the initial spin was 10.4, since 4.4 h otherwise exceeds their spin limit.

For every simulation performed, data was output every 1000 timesteps, providing detailed temporal resolution of changes to the body or binary system. The results presented below focus on the physical changes to the body before and after mass ejection, as well as the properties of any orbiting body.

6. RESULTS

Multiple simulations were run for each set of parameters but in the following, for the sake of brevity, we will often describe only a representative case. Nevertheless, many of the following plots and tables include results of the entire suite of simulations.

6.1 NOMINAL RUBBLE-PILE

A. Shape and Spin changes of the largest body

The shape of the largest body is followed continuously throughout the simulations, before and after mass loss. For the nominal case, where the aggregate behaves like material with an angle of friction ~40°, the shape changes the body undergoes are very similar to those predicted analytically for bodies constructed of cohesionless granular material (Holsapple 2001, 2004).

For the bodies starting as spheres, the first shape change begins at a spin rate of 2.9 h (see Fig. 5). The body spins to its minimum spin rate at ~2.8 h, at which time more re-shaping occurs, pushing the axis ratio *c/a* to ~ 0.8, while *b/a* stays near unity for the entire simulation. This re-shaping, where the *c/a* axis ratios adjust, is the start of the transition from spherical to

oblate. The long and intermediate axes, *a* and *b*, are nearly equal, while the short axis becomes significantly shorter than both. The next major re-shaping occurs at a similar time as the first mass loss, pushing the *c/a* value to ~0.65, where it stays for the rest of the simulation. At this set of axis ratios the body maintains a spin rate ~2.9–3.0 h, and loses mass steadily without more dramatic reshaping.

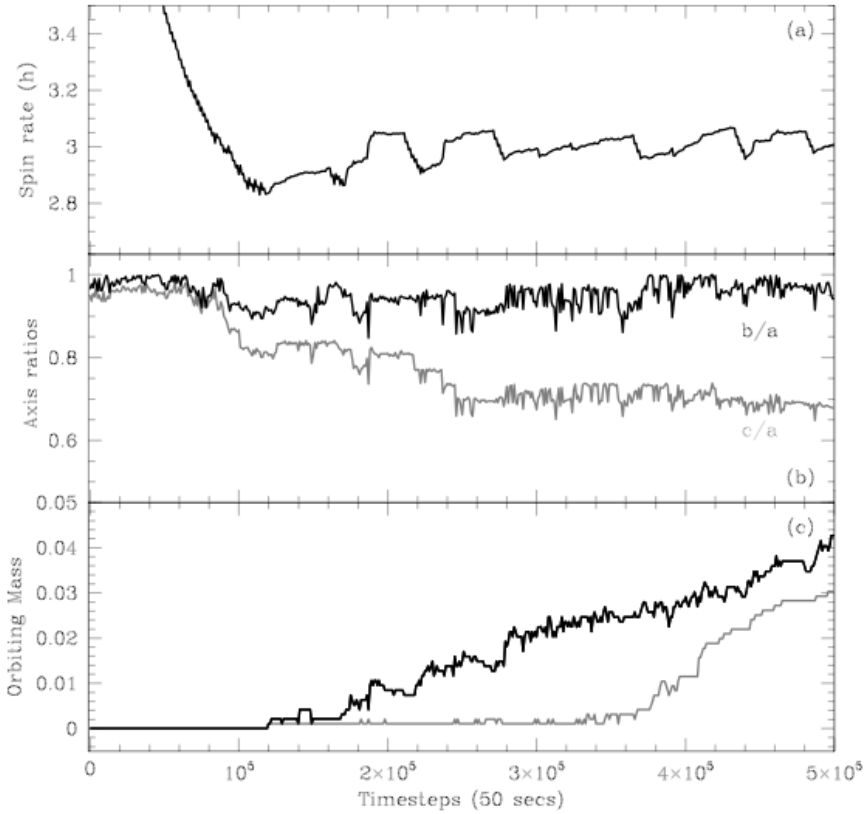

Figure 5: This plot shows (a) spin period in hours, (b) axis ratios *b/a* (black line) and *c/a* (grey line), (c) and the orbiting mass (black line) and mass of the largest satellite (grey line) as a function of 50 second timesteps for the nominal rubble pile spin-up case. This is the beginning of the simulation, focusing on the initial reshaping and first mass loss.

This state of rapid spin and oblate shape is easily compared to analytical models of equilibrium shapes and spin limits when the normalized angular momentum is compared with the axis ratios. This allows a comparison to the Jacobi/Maclaurin fiducials for fluid bodies as well as analytical determinations of limits for cohesionless granular material. Figure 5 shows the evolution of this body in this space, and shows the body holding equilibrium shapes well beyond those of the fluid limits, as observed by Richardson et al. (2005). Similarly, the re-shaping and mass loss are clearly associated with the boundaries for cohesionless material. The limiting axis ratios for material with ϕ~20° and ϕ~40° are shown on Fig. 6 (below), and the simulation plotted evolves into this regime before initiating mass loss or re-shaping.

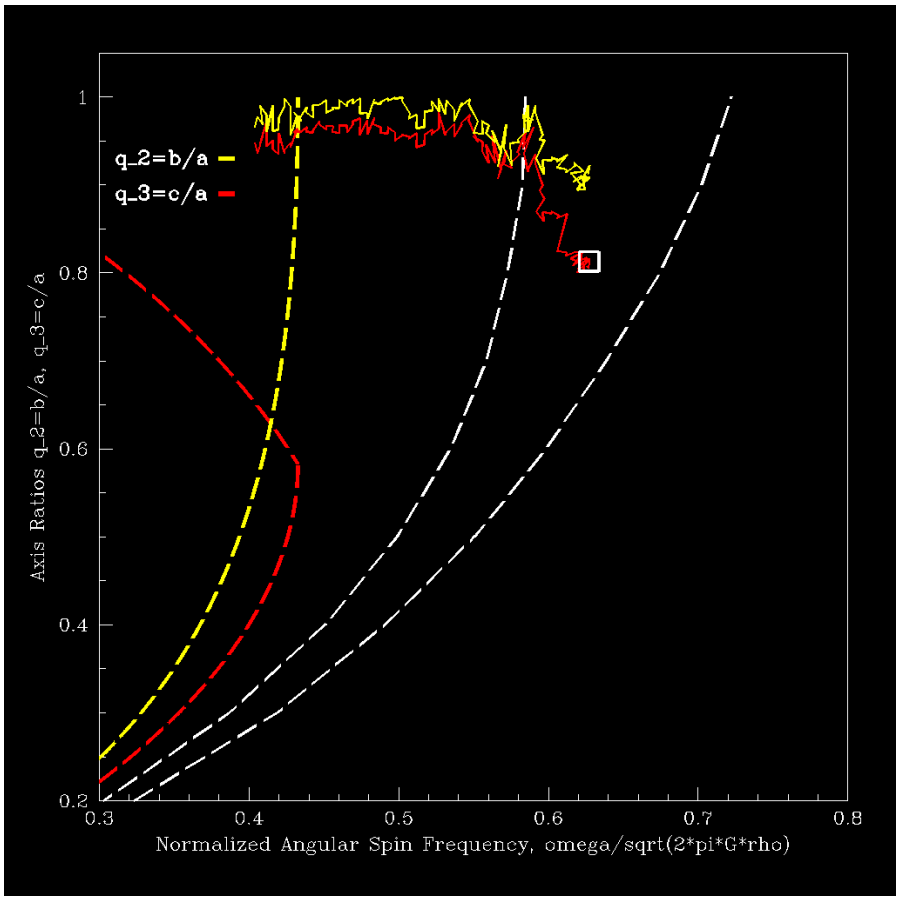

Figure 6: This figure shows the evolution of the axis ratios for the nominal rubble pile as the spin frequency is increased. The axis ratio *c/a* is plotted in red, while *b/a* is plotted in yellow. The red and yellow dashed curves are the Jacobi/Maclaurin limits for fluid bodies, and the colors correspond to the same axis ratios as for the rubble pile. The left dashed white line is the spin limit for a cohesionless granular material with an angle of friction of 20°, while the right dashed white line is the same but for a material with angle of fricton 40°. Values of the axis ratios are on the y-axis, and the x-axis is normalized spin frequency. The open white square indicates that mass was lost at that point in the evolution.

B. Mass-loss and satellite formation

A specific study of satellite formation performed under this contract is the subject of an article published in the journal *Nature* on July 10th, 2008 (Walsh, Richardson, Michel, 2008, *Nature* **454**, 188-191) with acknowledgments to this Ariadna contract and we refer the interested reader to this paper for more details.

As noted above, mass loss begins soon after the body becomes slightly oblate (shown in Fig. 5 at timestep 1.2×10^5, and by the white square in Fig. 6). The first mass that is ejected comes from the equator (see Fig. 7). Mass loss following this event continues from similar areas near the equator. The ejected mass accumulates into a satellite for some of the tested properties with this nominal case, and is strongly dependent on the coefficient of restitution of the material in the simulation. For the lowest value of restitution coefficient tested, 0.2, satellite accumulation is very efficient: all ten simulations had more than 90% of the ejected mass accumulate into a satellite. Higher values of restitution coefficient proved less efficient at forming satellites, and for values above 0,6, no satellite formation occured.

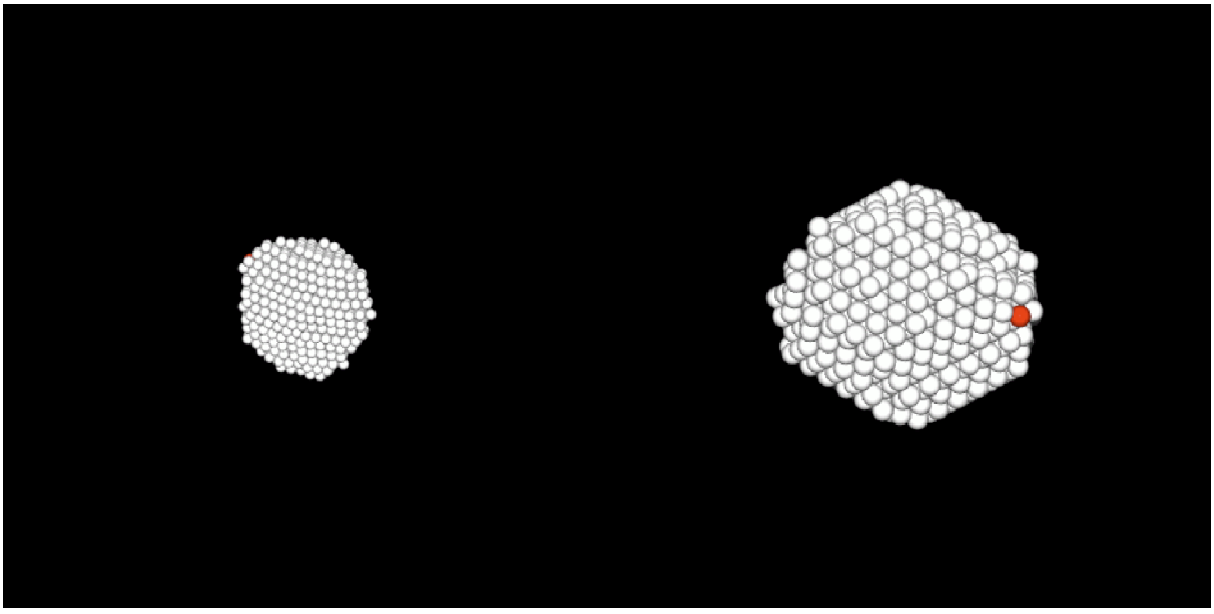

Figure 7: Two views of the rubble pile immediately preceding first mass loss. The red particle is the first particle to be ejected. The left panel shows an overhead view, looking down the spin axis of the body, and the right panel shows an equatorial view of the body.

C. Satellite properties and orbit

When satellite formation occurs, the systems initially have very small semi-major axes, with secondary orbits only marginally above the surface of the primary. The first satellites do not form until there is a significant amount of mass already in a close orbit around the largest body. After only a few particles have accumulated most of the remaining orbiting debris is quickly accreted (as seen in Fig. 4, where ~2.5% of the mass is in orbit before the first large satellite forms, and then it accumulates nearly all the orbiting mass quickly). Satellite formation then continues with high efficiency until the mass of the secondary nears the mass of the primary (Ms > 0.5 Mp), at which point our simplified model of YORP likely breaks down (see below).

The properties of the secondaries are a strong function of when the simulations are stopped. The spin-up of the main body is artificially imposed and does not depend on the changing shape of the body, or the ejection of mass. However, among the observed population of binaries, only one is known to have a secondary exceeding 50% the size of the primary. So there is likely a mechanism that stops mass from being transferred to the secondary. The moment in time at which this happens is unclear, and therefore it is difficult to determine at what point our simulations should be compared with the actual observed binary population. For consistency, we analyze secondaries when they have become 30% the size of the primary. This decision was based on work by Cuk (2007), in which it was estimated that the BYORP (Binary-YORP) effect would begin to dominate at this size, halting mass transfer. Cuk (2007) analysed the relative timescales between the YORP effect and the BYORP effect. The BYORP effect is a thermal effect similar to YORP which acts on a synchronized binary system rather than simply a single body, where the secondary acts as a level arm for administrating torques. The former (YORP) is dependent only on the size, shape and orbit of the primary. The BYORP effect is more complex and depends on the relative sizes of the primary and secondary, their mutual orbit, and the spin states of both. The estimate derived

for when the BYORP effect becomes dominant is when the secondary is about 30% the size of the primary.

The satellites created in our nominal case compare very favorably to the observed population of NEA binaries (Fig. 8). All secondaries formed in the simulations have very low eccentricity, below 0.2 in all cases. They also form with very close orbits typically between 2.5–4.5 R_p. This agrees well with the observed population of NEA binaries, which are all found with very close orbits (2.5–5 R_p) and low eccentricities (with a few exceptions; Hermes, 1998 ST27).

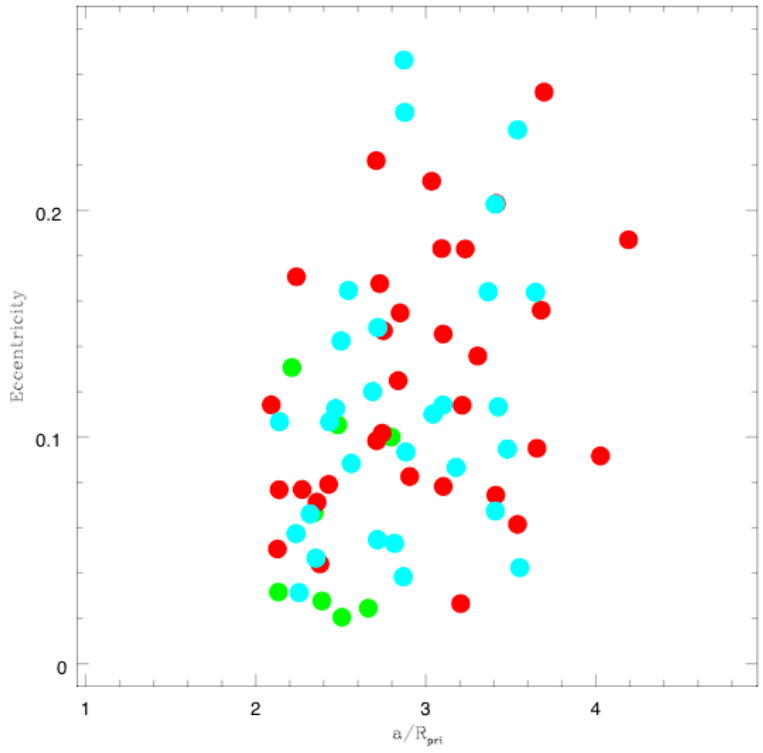

Figure 8: The properties of secondaries formed in different simulations, shown as eccentricity *vs*. orbital semi-major axis in units of primary radii (R_p). The red circles are binaries formed in the intermediate cases, the cyan circles are for those formed in the nominal cases, and the green are formed from piles with cores.

The material that forms the secondary originates primarily on the surface of the progenitor asteroid. To quantify the specifics of surface material transfer, we color-coded original surface particles in our nominal, low coefficient of restitution simulations (see Fig. 9). The results showed that 70–90% of the particles in the secondary were originally surface particles on the primary. Also, 15–35% of the surface of the primary are uncovered particles, which did not originate at the surface.

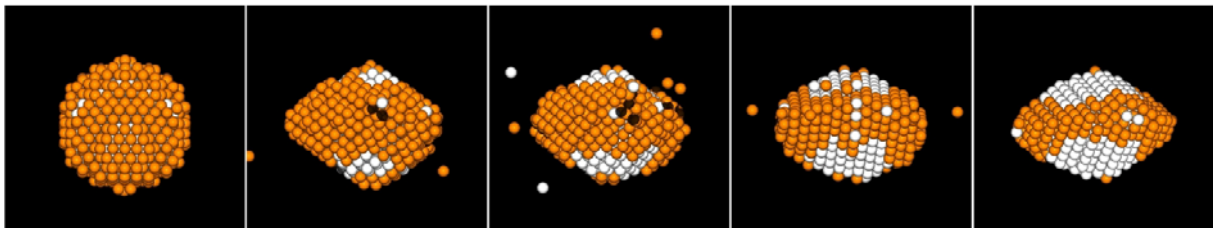

Figure 9: Snapshots of the evolution of surface material during spin-up, mass-loss and satellite formation. The panes from left to right follow the evolution of the primary body through satellite formation. The orange particles are initially surface particles and the white particles are originally interior particles (from Walsh, Richardson, Michel, 2008, *Nature* **454**, 181-191).

6.2 INTERMEDIATE CASE

A. Shape and Spin changes of the largest body

The intermediate case was designed to have properties placing it somewhere between the nominal case and the fluid case. This should allow the bodies to deviate from the fluid limits and maintain less extremely elongated shapes at critical spin rates and mass loss. The evolution of these rubble piles shows that the piles are indeed an intermediate case, as they do not immediately re-shape to fluid shapes. However, as the simulations progress, and the body is pushed to more rapid spin rates, the body re-shapes and loses mass beyond the fluid limits, but before they reach the 20° angle of friction limits (see Fig. 10). The first mass loss occurs just as the *c/a* axis ratio reaches the 20° limit. At this point the axis ratios are 1:0.8:0.45. As the simulation progresses, the body does not continue to get more elongated, and instead maintains a constant shape.

The simulations of these rubble piles do show substantial elongations, though the *b/a* axis ratio never exceeds 1:0.8. The average axis ratios for the length of the simulation stay very near those at which first mass loss occurs.

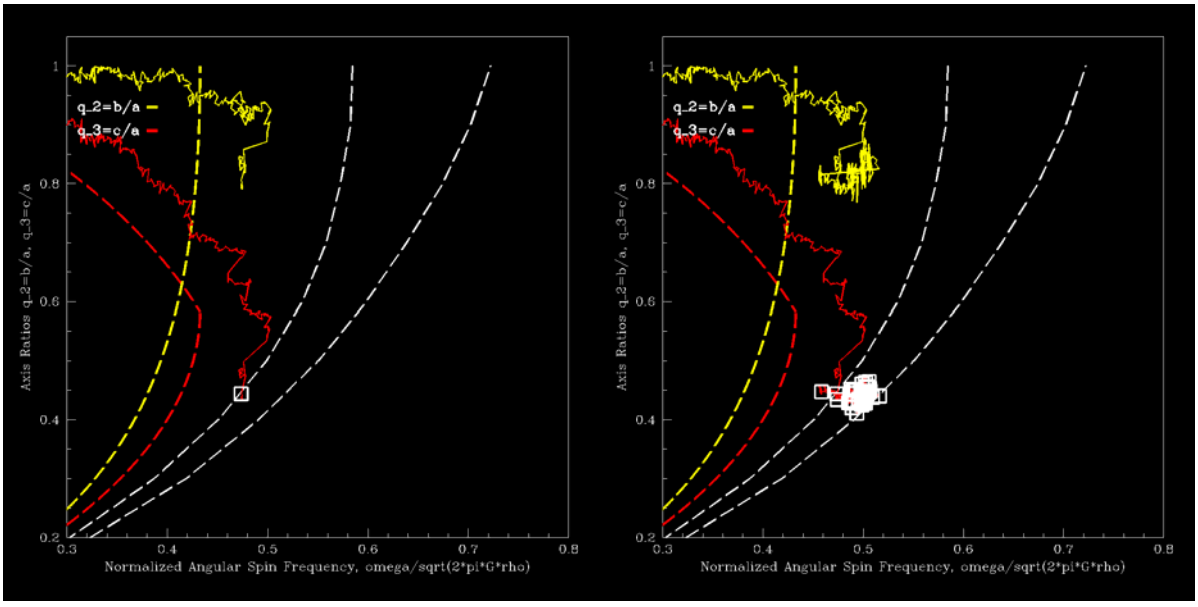

Figure 10: On similar axes as described in Fig. 5, we plot the evolution of the axis ratios for the intermediate rubble pile case. The left pane shows the evolution up to the point of mass loss, which happens very close to the 20° angle of friction limit. The right pane shows the long-term evolution of the body, with the shape of the rubble pile not deviating much through many subsequent episodes of mass loss.

B. Mass-loss and satellite formation

The shape of the bodies at mass loss for the intermediate case is tri-axial, with a moderate equatorial elongation. The first mass loss does not occur until significant re-shaping has occurred and the body has achieved its most elongated axis ratios, approximately 1:0.8:0.4. This occurs at roughly timestep 300,000 (where timesteps are ~50s), after gradual reshaping began at timestep 100,000 (see Fig. 11). The spin period at this first mass loss is ~3.5 h.

The satellite accumulation is delayed until ~7% of the total system mass is in orbit around the primary body. Similarly to the nominal case, once the satellite formation begins, it rapidly gains mass, efficiently accumulating ejected material.

The intermediate case was not always favorable for satellite formation, and in many cases did not form any satellites. The maximum equatorial elongations attained in these cases are less extreme than the following fluid cases, but much more extreme than the nearly spherical/oblate shapes created in the nominal case. These intermediate cases indicate a limiting equatorial elongation required for satellite accumulation, which appears to be somewhere around 1:0.8 for the *a:b* axis ratio.

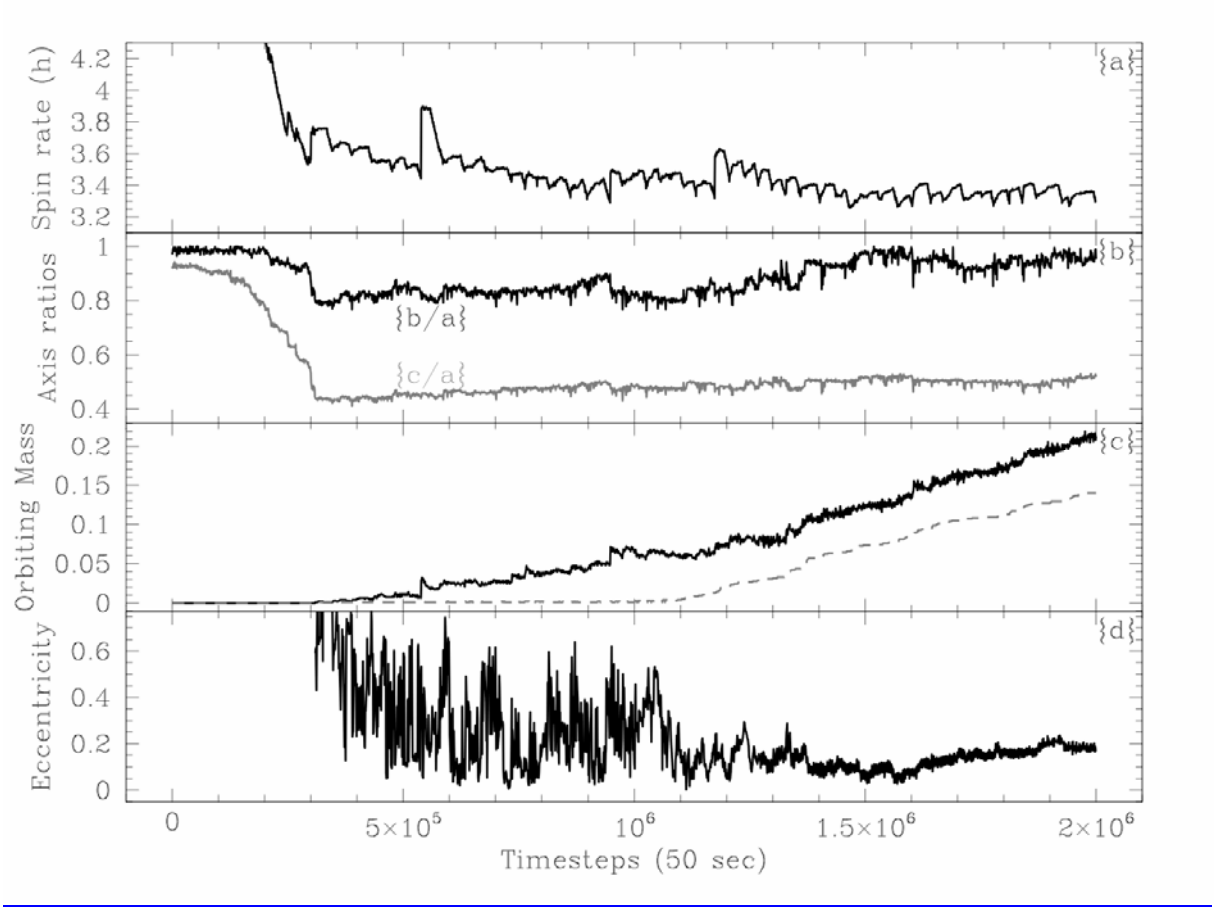

Figure 11: Evolution of (a) spin rate, (b) axis ratios, (c) orbiting mass and largest satellite, and (d) eccentricity of the largest satellite as a function of time in 50 sec. timesteps. See Fig, 4 for explanation of quantities plotted.

6.3 FLUID CASE

A. Shape and Spin changes of the largest body

The fluid case behaves nearly as theory would predict an inviscid fluid would under the spin-up process described. At the outset of the simulation the body adjusts to a shape and spin state near the fluid equilibrium. Analytical descriptions of a classical fluid, with the initial spin of 10.4 h, suggest that neither a spherical nor a 2:1:1 prolate shape is stable. As the spin is increased, the body continues to move to the right on the plot (Fig. 12 below), reaching the position of maximum spin frequency for a fluid, near the bifurcation point where a Maclaurin ellipsoid becomes tri-axial and becomes a Jacobi ellipsoid.

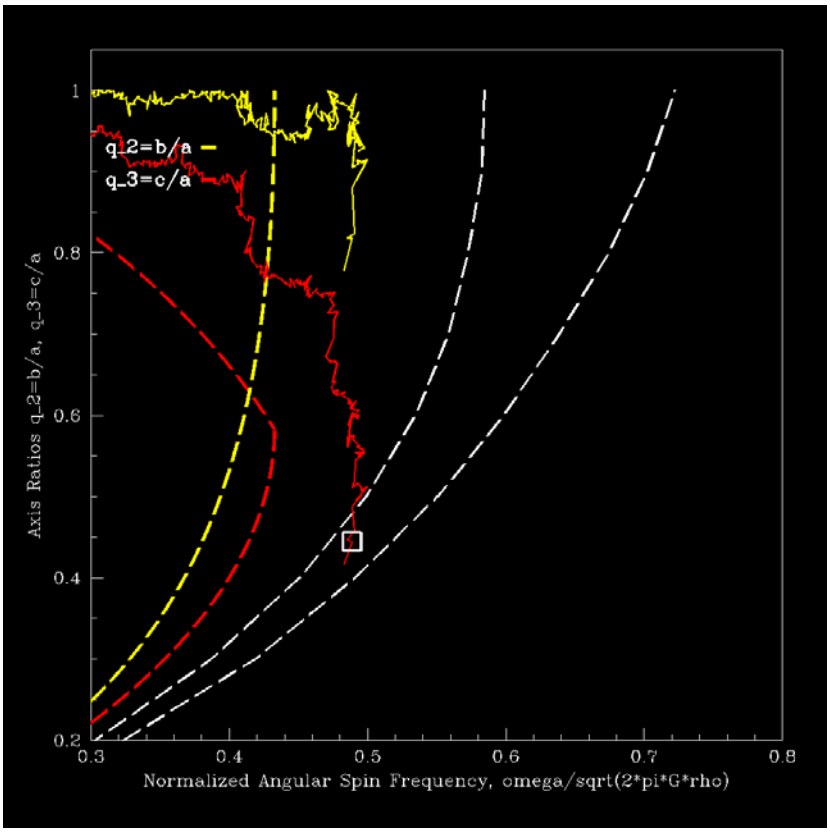

Figure 12: Evolution of a fluid-like rubble pile, which follows a trajectory on this plot quite different from the nominal case (c.f. Fig. 5): neither axis ratio (*b/a* in yellow, *c/a* in red) strays very far from the Maclaurin/Jacobi limits (where the yellow dashed line is the limits for *b/a* and the red dashed line is the limit for *c/a*).

The average shape and spin rate that the fluid-like body maintains for the bulk of each simulation is a tri-axial ellipsoid with axes of roughly 1:0.65:0.4 with a rotation period ~4 h. This configuration is closely in line with the Jacobi ellipsoid for a body with bulk density of 2.0 g/cc (Fig. 13).

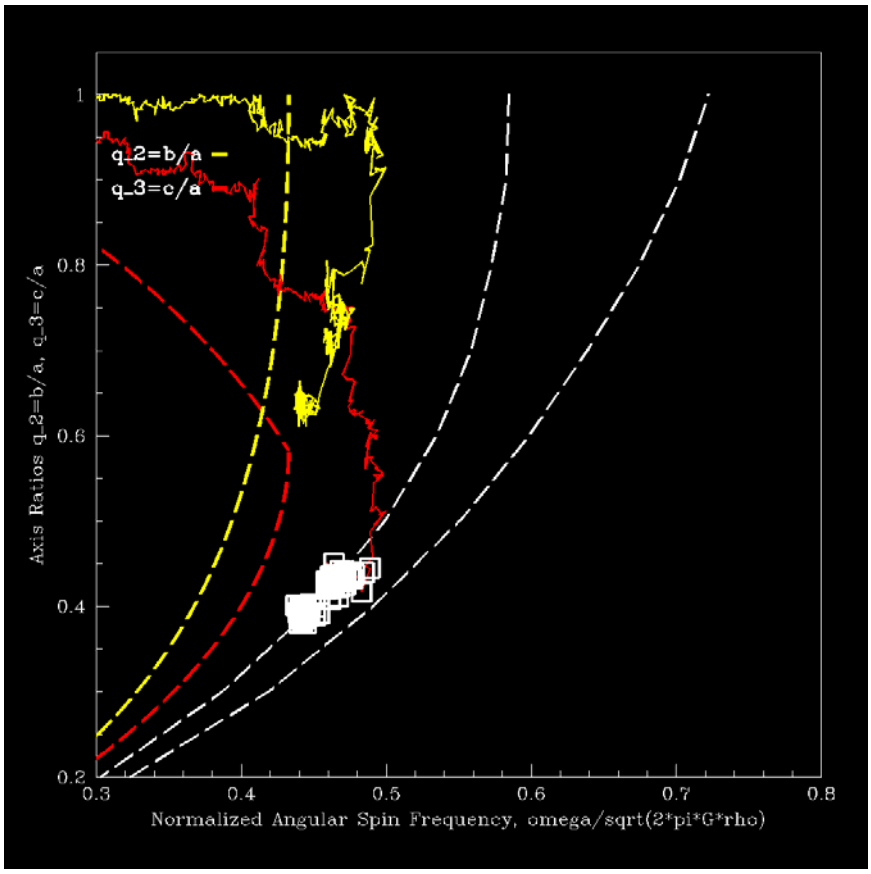

Figure 13: An extension of Fig. 12 to later time, showing the long-term evolution of the spin and shape of the fluid-like rubble pile. Both body axis ratios progress towards the Jacobi/Maclaurin limits. Note that we cannot model perfectly fluid bodies, which is why the ratios do not reach the fluid line, although they progress towards them.

B. Mass-loss and satellite formation

Mass loss begins after major re-shaping has occurred. The mass loss proceeds generally in the manner of single particles released from the end of the long axis of the near-equilibrium triaxial shape it attains. This triaxial shape frustrates satellite formation for all values of coefficient of restitution tested. The body typically has an equatorial elongation of 2.5 (see Fig. 14), which causes significant perturbations in its vicinity.

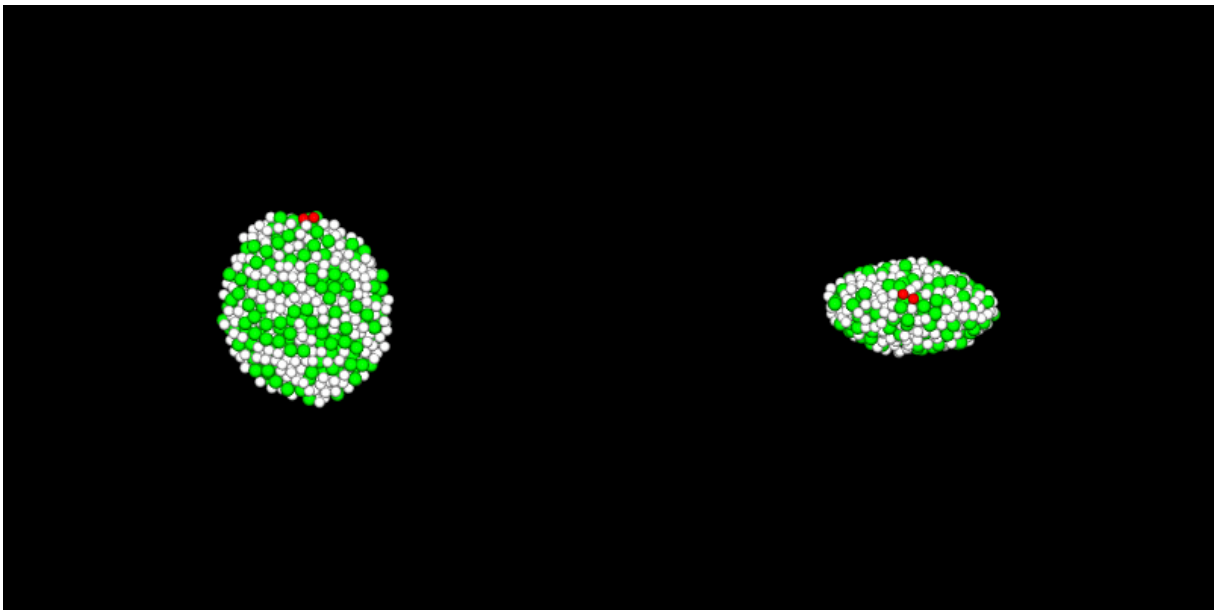

Figure 14: The first two particles ejected from the surface of the fluid-like rubble pile. The left pane is an overhead view looking directly down the spin axis of the body, and the right pane is an equatorial view. The green particles are 25% larger than the white particles, and the two red particles are the first two ejected off the surface. After this first mass loss the body continues to evolve to even more elongated shapes.

Only a few fluid-like cases were observed to lose a significant number of particles at once, and most originate from a highly elongated pear-shaped shape configuration. In this scenario the mass loss usually happens from the tapered end of the pear-shaped mass. However, none of the cases ever lose more than 5% of the mass in a single mass loss event.

6.4 CORES

A. Shape and Spin changes of the largest body

The evolution of the large-core models progressed in a manner similar to the intermediate case. The axis ratios evolved with the body staying oblate (so *b/a* stay constant, while *c/a* gets smaller) up through the first instance of mass loss (Fig. 15, 16). After the initial mass loss, the shape evolved slightly to attain average axis ratios of roughly 1.0:0.85:0.5. Despite the fluid-like flow of the exterior particles, the large cores restricted the overall elongation the body could attain. The cases with smaller cores behaved in a nearly fluid-like manner; in these cases the cores are insufficient to prevent the extreme axis ratios which are found in the fluid cases.

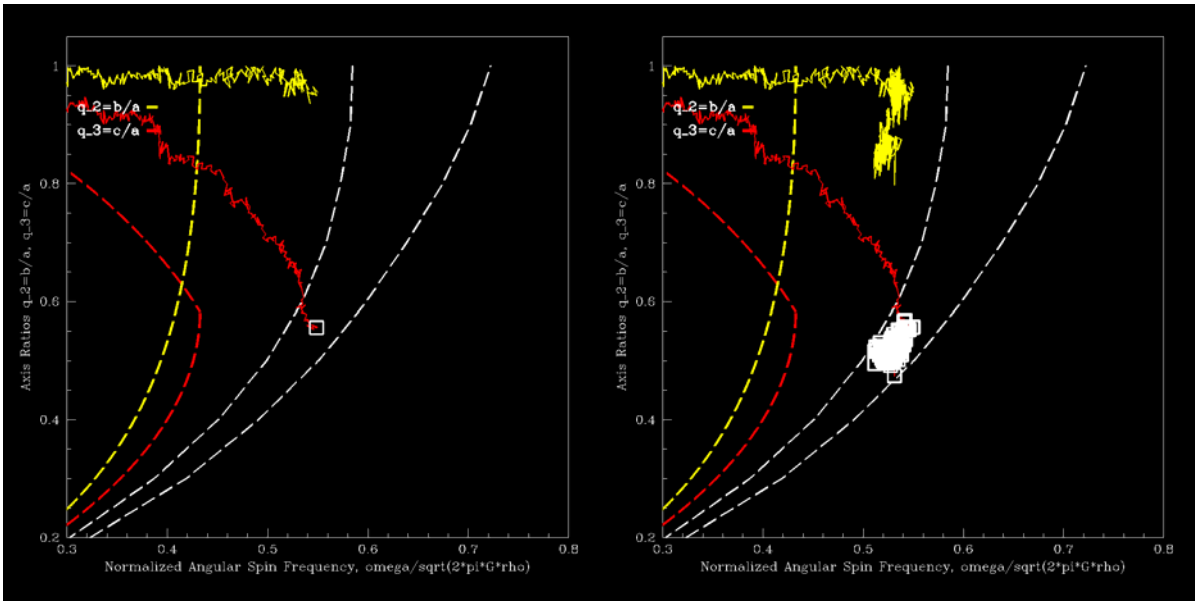

Figure 15: Evolution of axis ratios as a function of the normalized angular spin frequency for an example case of a rubble pile with a rigid core. The first mass loss occurs beyond the 20° angle of friction limit, and throughout the simulation the equatorial elongation stays low, ~1:0.85.

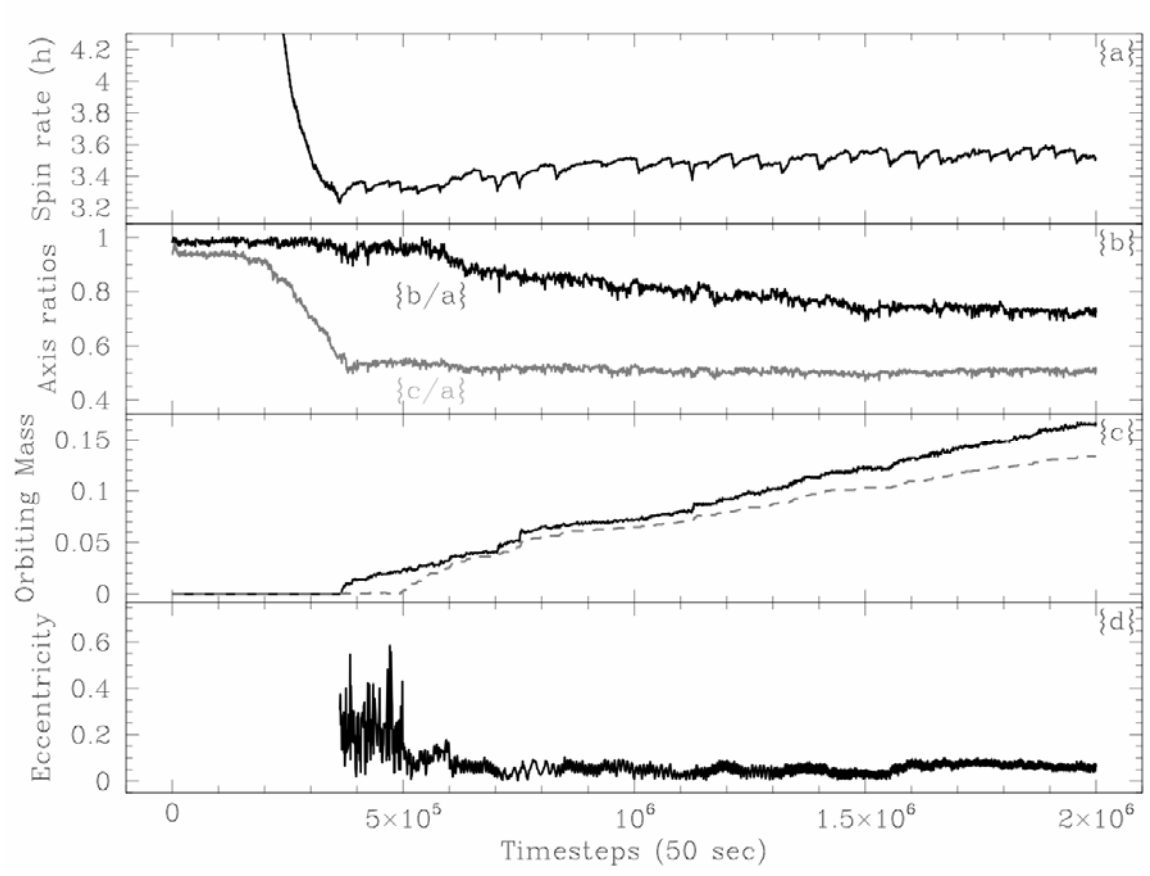

Figure 16: Evolution of (a) spin rate, (b) axis ratios, (c) orbiting mass, and (d) eccentricity of the largest orbiting mass, for the case of a rubble pile with a large rigid core.

B. Mass loss and satellite formation

Mass loss is only found in the simulations with a large core. Again, the relationship between equatorial elongation and successful satellite formation is critical, and the small core simulations flow in a fluid-like manner to take very elongated shapes (see Fig. 17). The large core simulations produce satellites as the maximum elongations rarely exceed ratios of *a:b* more extreme than 1:0.8.

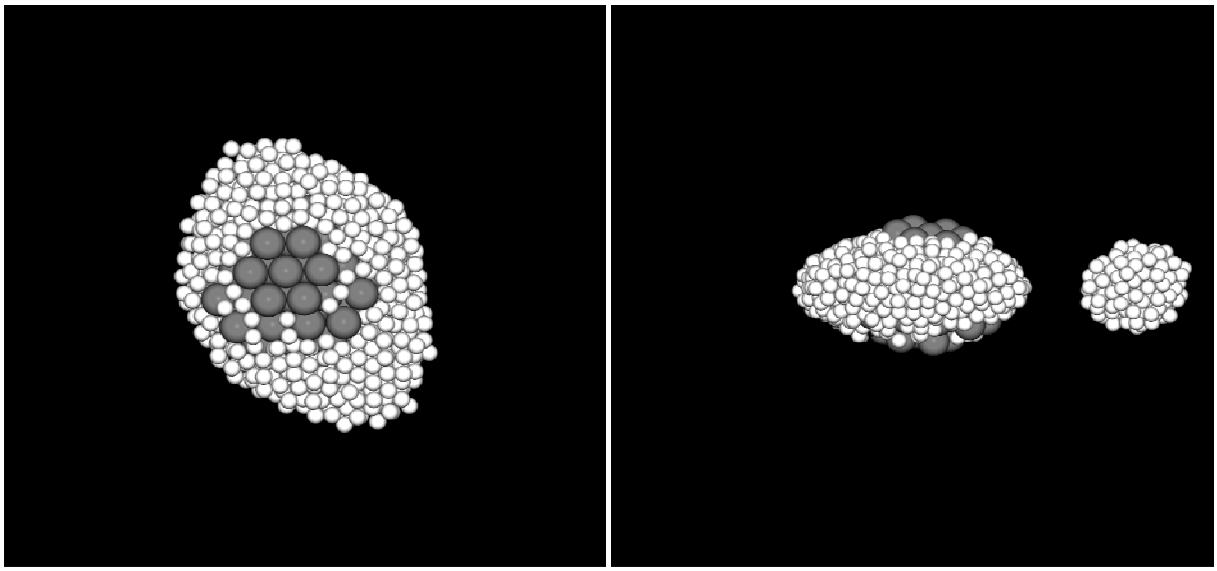

Figure 17: Snapshots from (left) above, looking down the spin axis of the primary, and (right) from the side, looking at the equator of a well-evolved binary system formed by spin-up of a rubble with a large rigid core. The gray particles are the inner core particles, and the white particles are the original surface particles.

6.5 TABLE OF SUMMARY OF RESULTS ON SATELLITE FORMATION

The following table summarizes the main cases of rotational fragmentation which resulted in the production of a small satellite. The bodies started as spherical (initial elongation of 1) or prolate (initial elongation of 2), with a 40° angle of friction (Nominal) or a 20° angle of friction (Intermediate) or as cores surronded by smaller particles (Core). None of the 0° angle of friction bodies (fluid cases) generated a satellite which is why they do not appear in this table.

Initial Elongation	Rubble Pile Type	Coefficient of Restitution	Largest Satellite M_{sec}/M_{pri}	Semi-Major Axis a/R_{pri}	Eccentricity	Timesteps ~50secs	Eq. Elongation final a/b	Elongation final a/c
1	Nominal	0,2	2,71%	2,545	0,165	452 000	1,048	1,475
1	Nominal	0,2	2,77%	2,562	0,088	504 000	1,200	1,499
1	Nominal	0,2	2,74%	2,816	0,053	424 000	1,108	1,490
1	Nominal	0,2	2,88%	2,255	0,031	447 000	1,007	1,440
1	Nominal	0,2	2,74%	3,408	0,203	383 000	1,002	1,424
1	Nominal	0,2	2,87%	3,552	0,042	1 731 000	1,039	1,588
1	Nominal	0,2	2,74%	2,687	0,120	499 000	1,095	1,111
1	Nominal	0,2	2,77%	2,434	0,107	532 000	1,031	1,491
1	Nominal	0,2	2,72%	2,718	0,148	939 000	1,029	1,490
1	Nominal	0,2	2,74%	3,426	0,113	441 000	1,036	1,484
1	Nominal	0,4	2,74%	2,883	0,093	414 000	1,037	1,467
1	Nominal	0,4	2,72%	2,501	0,142	621 000	1,104	1,452
1	Nominal	0,4	2,76%	3,179	0,087	770 000	1,013	1,435
1	Nominal	0,4	2,75%	3,645	0,164	426 000	1,012	1,438
1	Nominal	0,4	2,91%	2,469	0,113	764 000	1,136	1,535
1	Nominal	0,4	2,84%	2,320	0,066	412 000	1,014	1,448
1	Nominal	0,4	2,72%	2,872	0,266	669 000	1,016	1,374
1	Nominal	0,4	2,96%	2,236	0,057	441 000	1,044	1,494
1	Nominal	0,4	2,72%	3,100	0,114	632 000	1,038	1,306
1	Nominal	0,6	2,78%	3,480	0,095	777 000	1,050	1,429
1	Nominal	0,6	3,31%	3,042	0,110	1 107 000	1,051	1,378
1	Nominal	0,6	2,80%	2,715	0,055	561 000	1,120	1,490
1	Nominal	0,6	2,78%	2,354	0,047	515 000	1,200	1,410
1	Nominal	0,6	2,72%	2,868	0,038	648 000	1,095	1,405
1	Nominal	0,6	2,83%	3,409	0,067	1 182 000	1,098	1,491
1	Nominal	0,6	2,77%	2,139	0,107	1 492 000	1,029	1,488
1	Nominal	0,6	2,82%	3,540	0,236	830 000	1,094	1,502
1	Nominal	0,6	2,73%	3,367	0,164	901 000	1,070	1,406
1	Nominal	0,6	2,81%	2,876	0,243	822 000	1,108	1,485
2	Nominal	0,2	2,84%	2,287	0,089	1 907 000	1,041	1,462
2	Nominal	0,2	2,75%	2,288	0,044	2 106 000	1,017	1,460
2	Nominal	0,2	2,75%	2,962	0,055	1 914 000	1,049	1,290
2	Nominal	0,2	2,76%	2,289	0,151	2 080 000	1,126	1,373
2	Nominal	0,2	2,80%	3,087	0,101	2 331 000	1,047	1,555
2	Nominal	0,2	2,85%	2,355	0,083	2 499 000	1,049	1,546
2	Nominal	0,2	2,74%	2,406	0,077	2 183 000	1,046	1,440
2	Nominal	0,2	2,73%	2,702	0,068	2 109 000	1,009	1,066
2	Nominal	0,2	2,77%	3,707	0,052	2 765 000	1,018	1,298
2	Nominal	0,2	2,76%	2,646	0,126	2 096 000	1,209	1,542
2	Nominal	0,4	2,77%	3,897	0,291	2 466 000	1,289	1,404
2	Nominal	0,4	2,73%	2,090	0,151	2 123 000	1,130	1,424
2	Nominal	0,4	2,81%	2,852	0,069	2 288 000	1,171	1,500
2	Nominal	0,4	3,04%	3,093	0,083	2 664 000	1,035	1,265
2	Nominal	0,4	2,75%	2,081	0,025	2 116 000	1,086	1,401
2	Nominal	0,4	2,72%	2,860	0,167	2 047 000	1,151	1,487
2	Nominal	0,4	2,82%	2,576	0,034	2 152 000	1,075	1,363
2	Nominal	0,4	2,84%	2,668	0,185	2 407 000	1,088	1,446
2	Nominal	0,4	2,79%	3,133	0,033	2 327 000	1,027	1,359
2	Nominal	0,6	2,54%	3,403	0,124	3 000 000	1,035	1,197
2	Nominal	0,6	2,73%	3,116	0,065	2 657 000	1,216	1,396
2	Nominal	0,6	2,75%	2,437	0,150	2 587 000	1,271	1,469
1	Intermediate	0,2	2,89%	2,429	0,079	1 209 000	1,050	1,933
1	Intermediate	0,2	2,79%	2,905	0,083	836 000	1,095	1,653
1	Intermediate	0,2	2,74%	3,093	0,183	1 383 000	1,026	1,630
1	Intermediate	0,2	2,79%	2,127	0,051	1 120 000	1,018	1,591
1	Intermediate	0,2	2,81%	2,091	0,114	1 870 000	1,108	1,907
1	Intermediate	0,2	2,76%	3,034	0,213	587 000	1,010	1,561
1	Intermediate	0,2	2,78%	2,729	0,168	1 110 000	1,011	1,530
1	Intermediate	0,2	2,79%	2,272	0,077	551 000	1,059	1,635
1	Intermediate	0,2	2,91%	2,708	0,222	986 000	1,001	1,597
1	Intermediate	0,2	2,77%	3,696	0,252	1 011 000	1,004	1,499
1	Intermediate	0,4	2,87%	3,214	0,114	1 115 000	1,058	1,584
1	Intermediate	0,4	2,79%	3,232	0,183	1 066 000	1,001	1,533
1	Intermediate	0,4	2,72%	2,137	0,077	1 316 000	1,076	1,624
1	Intermediate	0,4	2,83%	3,654	0,095	1 648 000	1,052	1,643
1	Intermediate	0,4	2,71%	3,102	0,145	617 000	1,010	1,716
1	Intermediate	0,4	2,73%	2,743	0,102	1 064 000	1,017	1,599
1	Intermediate	0,4	2,94%	3,103	0,078	906 000	1,015	1,567
1	Intermediate	0,4	2,76%	4,192	0,187	1 045 000	1,011	1,573
1	Intermediate	0,6	2,72%	4,027	0,092	1 288 000	1,003	1,517
1	Intermediate	0,6	2,75%	3,411	0,074	1 223 000	1,014	1,550
1	Intermediate	0,6	2,71%	3,205	0,027	1 795 000	1,031	1,559
1	Intermediate	0,6	2,75%	2,751	0,147	1 966 000	1,091	1,595
1	Intermediate	0,6	2,77%	2,378	0,044	1 132 000	1,078	1,496
1	Intermediate	0,6	2,70%	3,539	0,061	1 406 000	1,077	1,625
1	Intermediate	0,6	2,81%	2,239	0,171	1 434 000	1,011	1,615
1	Intermediate	0,6	2,81%	2,711	0,098	1 482 000	1,090	1,575
1	Intermediate	0,2	2,91%	2,848	0,155	1 755 000	1,007	1,525
1	Intermediate	0,2	2,71%	3,414	0,203	1 656 000	1,326	1,737
1	Intermediate	0,4	2,84%	3,305	0,136	1 965 000	1,159	1,770
1	Core	0,2	2,71%	2,212	0,131	701 000	1,202	1,890
1	Core	0,2	2,74%	2,797	0,100	1 674 000	1,245	1,371
1	Core	0,2	2,46%	2,133	0,032	2 000 000	1,320	1,432
1	Core	0,2	2,72%	2,506	0,021	763 000	1,274	1,310
1	Core	0,2	2,72%	2,389	0,028	1 740 000	1,161	1,410
1	Core	0,2	2,73%	2,344	0,067	1 400 000	1,269	1,365
1	Core	0,2	2,32%	2,662	0,025	2 000 000	1,218	1,353
		Average	2,77%	2,847	0,110	1 356 092	1,084	1,491
		Minimum	2,32%	2,081	0,021	383 000	1,001	1,066
		Maximum	3,31%	4,192	0,291	3 000 000	1,326	1,933

7. AN ATTEMPT TO SIMULATE A SPIN-UP USING AN ARTIFICIAL WEDGE

Some tests were attempted where the angular momentum increases were supplied by an object, or "wedge", embedded in a rubble pile. The motivation to do these tests was to relate this study to a space mission whose purpose would be to increase artificially the spin of an asteroid using such kind of tool.

The wedge was constructed out of particles identical to those in the rubble pile, but were bonded together to form a rigid body. This rigid construction was then embedded into a rubble pile during the collapse phase of rubble pile formation (see Fig.18). This process presented the first major problem with this technique, as the insertion of the wedge was very dependent on the actual shape of the wedge, with some falling over, or simply sitting on the surface. The nature of the model rubble piles was not conducive to supporting a large rigid structure embedded into its surface. The next problem was the actual integration of the spin-up of the rigid wedge, as this employed a relatively new functionality in the code, which did not perform well in the regime of YORP simulations (2 million timesteps or more). Therefore, we had to give up performing these tests. However, these attempts showed that simulating such a concept is not an easy task, and a real space mission using such a tool would have to deal with many more difficulties. In particular, interacting with the surface of a small body and implementing such a tool at a given depth requires a method to deal with small gravity and to have some good guess on the surface properties (strength, regolith thickness etc …).

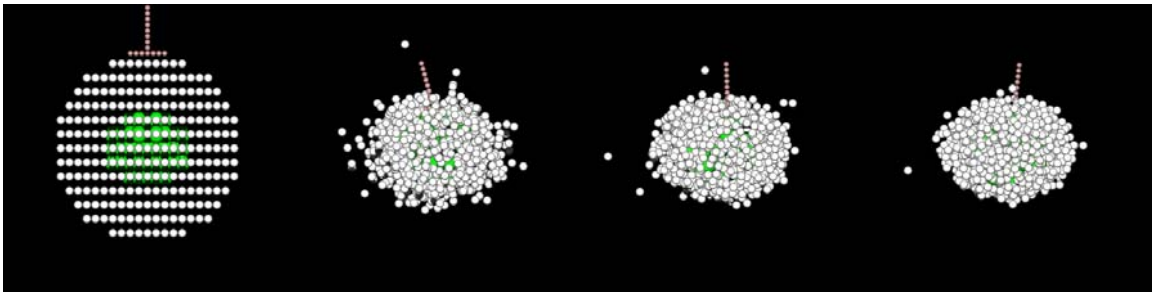

Figure 18: Snapshots (from left to right, looking at the equator) of the artificial spin-up of a rubble pile with a core (green partciles) using a rigid wedge made of spherical pink particles identical to those in the rubble pile. One can see that the wedge, once implemented cannot stay stable, preventing us to represent the expected artificial spin-up using such a concept.

8. CONCLUSIONS

The main scientific conclusions of our study of rotational fragmentation are the following:

- Shape change at rapid rotation rates for asteroids depends strongly on the internal construction of the body. Best estimates for asteroidal material, based on the existence of binaries, would suggest similarity to our nominal case with an angle of friction ~ 40 deg, or our case of a large rigid core. Both of these cases remain spherical/oblate up through first mass loss, and generally permit satellite formation. The spin rate at which first re-shaping and mass loss occurs depends strongly on asteroid density and initial shape, but for usual near-spherical shapes and densities, spin periods below 4 h are where first mass loss should occur.

- Mass loss will occur at or near the equator of a rapidly rotating asteroid. As the body re-shapes and evolves, mass flows to the equator, and in our nominal case creates a ridge from which material is ejected into orbit. This means that in general the movement of material on the surface is from the poles to the equator.
- Binaries that have formed from slow spin-up (presumably via the YORP effect), will likely have a significant portion of their surface removed and have subsurface material uncovered. In our simulations the poles are areas where material will be uncovered first, and much of the moved surface material is what constitutes the satellite.
- Satellite formation in a slow spin-up scenario depends on the asteroid's ability to maintain low equatorial elongation, and for the asteroidal material to dissipate energy during collisions. The cases where large satellites formed were for the nominal and large-core tests with coefficients of restitution below 0.6. The intermediate cases also formed satellites, though with less efficiency than the nominal or core cases. The fluid-like cases generally never led to binary formation.

In the context of a space mission devoted to the disruption of a body by artificially spinning it up, the first conclusions we state above are the most important ones. We have characterized the way different body types behave under gradual spin-increase up to and beyond the point of mass loss. We have then characterized the movement and the escape of mass from the bodies, and the long term evolution of the ejected mass (whether it forms a satellite or not). The timescales of reshaping and mass loss will then depends on the spin-up rate imposed by the satellites and can be infered from our results.

9. REFERENCES

Abe S. et al. 2006. Mass and local topography measurements of Itokawa by Hayabusa. Science 312, 1344-1347.

Albert R., Albert I., Hornbaker D., Schiffer P. and Barabasi A.L. 1997. The maximum angle of stability in wet and dry spherical granular media. Phys. Review E 56, 6271-6274.

Asphaug E. and Benz W. 1994. Density of Comet Shoemaker–Levy 9 deduced by modelling breakup of the parent “rubble pile.” Nature 370, 120-124.

Benz, W. 1990. Smooth particle hydrodynamics: A review. In *Numerical Modeling of Nonlinear Stellar Pulsations. Problems and Prospects* (J. R. Buchler, Ed.), pp. 269–288. Kluwer Academic, Dordrecht.

Benz W. and Asphaug 1994. Impact simulations with fracture. I. Method and test. Icarus 107, 88-116.

Benz W. and Asphaug E. 1999. Catastrophic disruptions revisited. Icarus 142, 5-20.

Fujiawara A. et al. 2006. The rubble-pile asteroid Itokawa as observed by Hayabusa. Science 312, 1330-1334.

Cuk M. 2007. Formation and destruction of small binary asteroids. Astrophys. J. 659, l57-L60.

Grady D.E. and Kipp M.E. 1980. Continuum modelling of explosive fracture in oil shale. Int. J. Rock Mech. Min. Sci. Geomech. Abstr. 17, 147-157.

Holsapple K.A. 1993. The scaling of impact processes in planetary sciences. Ann. Rev. Earth Plan. Sci. 21, 333-373.

Holsapple K.A. 2001. Equilibrium configurations of solid cohesionless bodies. Icarus 154, 432-448.

Holsapple K.A ., Giblin I., Housen K., Nakamura A., Ryan E. 2002. Asteroid impacts: Laboratory experiments and scaling laws. In: Bottke Jr., W.F., Cellino, A., Paolicchi, P., Binzel, R.P. (Eds.), *Asteroids III*. Univ. of Arizona Press, Tucson, AZ, pp. 443–462.

Holsapple K.A. 2004. Equilbrium figures of spinning bodies with self-gravity. Icarus 172, 272-303.

Holsapple K.A. 2007. Spin limits of Solar System bodies : from the small fast-rotators to 2003 EL61. Icarus 187, 500-509.

Holsapple K.A. and Michel P. 2006. Tidal disruptions: a continuum theory for solid bodies. Icarus 183, 331-348.

Kaasalainen M. et al. 2007. Acceleration of the rotation of asteroid 1862 Apollo by radiation torques. Nature 446, 420-422.

Lawn B.R. and Wilshaw T.R. 1975. Fracture of brittle solids. Cambridge Univ. Press, New-York.

Leinhardt Z.M., Richardson D.C. and Quinn T. 2000. Direct *N*-body simulations of rubble pile collisions. Icarus 146, 133–151.

Leinhardt Z.M. and Richardson D.C. 2005. A fast method for finding bound systems in numerical simulations: Results from the formation of asteroid binaries. Icarus 176, 432-439.

Lowry S.C. et al. 2007. Direct detection of the asteroidal YORP effect. Science 316, 272-274.

Monaghan, J.J. 1992. Smooth particle hydrodynamics. Ann. Rev. Astron. Astrophys. 30, 543–574.

Nakamura A., Michel P., Setoh M. 2007. Weibull parameters of Yakuno basalt targets used in documented high-velocity impact experiments. J. Geophys. Res. 112, Issue E2, CiteID E02001.

Paddack S. J., and Rhee J.W. 1975. Rotational bursting of interplanetary dust particles. Geophys. Res. Lett. 2, 365–367.

Pravec P. and Harris A.W. 2000. Fast and slow rotation of asteroids. Icarus 148, 12-20.

Richardson D.C., Quinn T., Stadel J. and Lake G. 2000. Direct large-scale N-body

simulations of planetesimal dynamics. Icarus 143, 45-59.

Richardson D.C., Leinhardt Z.M., Melosh H.J., Bottke Jr. W.F., Asphaug E., 2002. Gravitational aggregates: evidence and evolution. In: Bottke Jr.,W.F., Cellino A., Paolicchi P., Binzel R.P. (Eds.), *Asteroids III*. Univ. of Arizona Press, Tucson, pp. 501–515.

Richardson D.C., Elankumaran P. and Sanderson R.E. 2005. Numerical experiments with rubble piles : equilibrium shapes and spins. Icarus 173, 349-361.

Richardson D.C., Michel P., Walsh K. and Flynn K.W. 2008. Numerical simulations of asteroids modelled as gravitationnal aggregates with cohesion. Plan. Space Sci., in press.

Rubincam D.P. 2000. Radiative spin-up and spin-down of small asteroids. Icarus 148, 2-11.

Taylor P.A. et al. 2007. Spin Rate of Asteroid (54509) 2000 PH5 Increasing Due to the YORP Effect. Science 316, 274.

Walsh J.B. 1965. The effect of cracks on the compressibility of rocks. J. Geophys. Res. 70, 381-389.

Walsh K. J., Richardson D.C. 2006. Binary near-Earth asteroid formation: rubble pile model of tidal disruptions. Icarus, 180, 201-216.

Walsh K. J., Richardson D.C. 2008. A Steady-State Model of Binary NEAs Formed by Tidal Disruption of Gravitational Aggregates. Icarus, 193, 553-566.

Walsh K. J., Richardson D. C., Michel P. 2008. Rotational breakup as the origin of small binary asteroids. Nature, 454 , 188-191.

Weibull W.A. 1939. A statistical theory of the strength of materials. Ingvetensk. Akad. Handl. 151, 5-45.